Applied Physics Letters

Direct measurements of thermal transport in glass and ceramic microspheres embedded in an epoxy matrix

Cite as: Appl. Phys. Lett. **119**, 023904 (2021); https://doi.org/10.1063/5.0055038
Submitted: 24 April 2021 • Accepted: 20 June 2021 • Published Online: 13 July 2021

Matthew F. Thompson, Xuewang Wu, Dingbin Huang, et al.

Applied Physics Letters ARTICLE scitation.org/journal/apl

Direct measurements of thermal transport in glass and ceramic microspheres embedded in an epoxy matrix

Cite as: Appl. Phys. Lett. **119**, 023904 (2021); doi: 10.1063/5.0055038
Submitted: 24 April 2021 · Accepted: 20 June 2021 ·
Published Online: 13 July 2021

View Online Export Citation CrossMark

Matthew F. Thompson,[1] Xuewang Wu,[1,a)] Dingbin Huang,[1] Yingying Zhang,[1] Nicholas C. A. Seaton,[2] Chi Zhang,[1] Matthew T. Johnson,[3] Jacob P. Podkaminer,[3] Victor Ho,[3] and Xiaojia Wang[1,b)]

AFFILIATIONS

[1]Department of Mechanical Engineering, University of Minnesota, Twin Cities, Minneapolis, Minnesota 55455, USA
[2]Characterization Facility, University of Minnesota, Twin Cities, Minneapolis, Minnesota 55455, USA
[3]3M Company, 3M Center, Saint Paul, Minnesota 55144, USA

[a)]**Present address:** Seagate Technology, Bloomington, MN 55455, USA
[b)]**Author to whom correspondence should be addressed:** wang4940@umn.edu

ABSTRACT

The time-domain thermoreflectance metrology is applied to evaluate the thermal conductivities of filler particles embedded in a composite matrix. Specifically, a system of glass and ceramic microspheres with a diameter of 100 to 150 μm embedded in an epoxy matrix was used as a representation of a typical composite thermal interface material (TIM) suitable for microelectronics applications. These measurements provide a direct characterization of the thermal properties of filler materials. The measured thermal conductivities of both borosilicate glass and yttria stabilized zirconia microspheres agree well with literature values for bulk materials, whereas the thermal conductivity of the alumina microspheres is nearly 50% lower than that of bulk crystals. The reduction in thermal conductivity of the alumina microspheres highlights how important this level of understanding is for TIM development and is attributed to enhanced phonon scattering due to structural heterogeneity, such as defects induced by phase mixing and microvoids. Combining sample preparation, structural characterization, and direct thermal measurements, our study reveals the structure–thermal property relationship for individual microspheres. The results of this work can facilitate the design and engineering of composite-based thermally conductive materials for thermal management applications.

Thermal management has attracted increasing attention as miniaturization of electronic devices drives higher energy density packaging. In many cases, thermal interface materials (TIMs) used to improve thermal transfer between rigid surfaces have become the limiting resistance.[1,2] TIMs often rely on composite structures of two or more constituent materials to achieve a desired suite of functionality (e.g., adhesion, mechanical strength, and electrical conductivity). A significant effort has been devoted to the engineering of TIMs for improved heat dissipation in microelectronics packaging. In these studies, a composite is created by loading a thermally conductive filler material into a host matrix to improve the overall heat removal.[3–9] However, many attempts to obtain high performance composites, particularly through the use of high thermal conductivity fillers, have resulted in lower than expected increases in the overall thermal performance.[10–12]

The effective thermal conductivity of composite materials depends on the thermal conductivity of the host medium, the thermal conductivity and volumetric fraction of the filler material, and the interfacial thermal conductance between the filler and the host. A variety of filler materials with different orientations and dispersion in composites have been experimentally examined.[8–10,13,14] However, most literature studies were only able to probe the effective thermal conductivities due to the challenges in direct measurements of small-size filler materials. Therefore, effective medium approximations (EMAs) are often used to calculate the thermal conductivity of composites for a comparison with measurement data.[15–18] However, in some cases, the EMA failed to accurately predict the effective thermal conductivities of composites. This discrepancy between model prediction and measurements can be partially attributed to the fact that the thermal conductivity values of bulk materials are often the only available

input for EMA or similar calculations. The manufacture and processing of fillers, however, can result in varying degrees of structural heterogeneity (e.g., microvoids, grain boundaries, crystalline phases), which may cause deviations from bulk properties.[19] A direct measure of true filler performance is absent in the field and would, therefore, be a benefit to the composite TIM material design process.

In this work, we investigate the thermal conductivity of borosilicate glass, yttria stabilized zirconia, and alumina microspheres. Borosilicate glass is chosen as a model system with an amorphous and fully dense structure and well-understood thermal conductivity. Yttria stabilized zirconia and alumina are inorganic filler materials with increasing structural complexity used in thermal composites due to their ease of manufacture and processing.[14,20,21] We prepared our samples by embedding the microspheres into an epoxy matrix and performing surface polishing. This enables us to conduct direct thermal measurements of individual microspheres using the time-domain thermoreflectance (TDTR) technique. The structure–thermal property relationship, revealed in this work, can be readily integrated into the design and optimization of currently existing composite-based thermally conductive products.

Three types of microspheres are studied in this work, including borosilicate glass microspheres, yttria stabilized zirconia (YSZ) microspheres, and alumina microspheres. Borosilicate glass (diameter: 125–150 μm) and YSZ (diameter: 106–125 μm) microspheres were purchased from Cospheric LLC, and alumina spheres (BAK120) were provided by Bestry. To prepare smooth sample surfaces necessary for TDTR thermal measurements, these microspheres were loaded into epoxy (EpoxySet®) forming composite disks with a high concentration of spheres located at the bottom of the disk. Both mechanical polishing and Focused Ion Beam (FIB) milling were employed to create flat and smooth surfaces on these microspheres. The mechanical polishing, illustrated in Fig. 1(a), was accomplished with a Buehler EcoMet® polisher and SiC abrasives with a manually applied light pressure, followed by a diamond paste. The high yield of mechanical polishing produces an epoxy disk (≈3 cm in diameter) that contains hundreds of microspheres with sufficiently smooth surfaces for TDTR measurements. FIB polishing was used for the surface preparation of alumina spheres due to their relative hardness, which complicates mechanical polishing [Fig. 1(b)]. The yield of FIB polishing was much lower due to the small area of interaction. Ultimately, mechanical polishing for long periods (∼12 h) produced the best results for high-throughput sample preparation for all three sample types.

The surface morphologies of all three types of microspheres were characterized with tapping-mode atomic force microscopy (AFM). The crystallographic phases and density of alumina spheres were measured with x-ray powder diffraction (XRD) and a helium gas pycnometer to estimate the porosity. The yttria concentration of YSZ microspheres was determined with the energy-dispersive x-ray spectroscopy (EDS). All samples are cleaned with nitrogen gas prior to transducer deposition.

The ultrafast laser-based TDTR metrology was used to measure the thermal conductivity of microspheres. The details regarding the TDTR setup can be found elsewhere.[22–27] A 5× objective lens with a $1/e^2$ radius of ≈12 μm was used for glass and YSZ microspheres. A 10× objective lens with a $1/e^2$ radius of ≈6 μm was used for alumina spheres because of their relatively rough surfaces with only localized smooth regions. Prior to thermal measurements, a thin film of aluminum (≈70 nm, Al) was sputtered onto the sample surface. This film serves as the light absorber and temperature transducer. The sample configuration is shown in Fig. 2(a). The sphere location was identified with a charged-coupled device (CCD) camera, as illustrated in Figs. 2(b)–2(d). During measurements, the pump and probe powers were carefully tuned to ensure that the steady-state temperature rise is less than 20 K for all samples.[22]

TDTR measurements produce an in-phase signal (V_{in}) and an out-of-phase signal (V_{out}). The V_{in} signal is proportional to the time evolution of the temperature change in the Al transducer film.[28–31] The V_{out} signal can be treated as the imaginary part of the frequency-domain temperature response of the sample at the modulation frequency.[22,32] We analyzed the ratio of $-V_{in}/V_{out}$ to increase the robustness of data reduction by fitting the ratio signals to a 3D thermal diffusion model in the cylindrical coordinates.[22,32] At short time delays, V_{in} also contains picosecond acoustics resulting from strain wave propagation within the Al transducer, which can be used to determine the thickness of the Al layer.[33]

The thermal model contains multiple parameters, such as the thickness, volumetric heat capacity, thermal conductivity of the Al transducer layer (h_{Al}, C_{Al}, Λ_{Al}), the microsphere (h, C, Λ), the interfacial thermal conductance (G) between the Al transducer layer and the

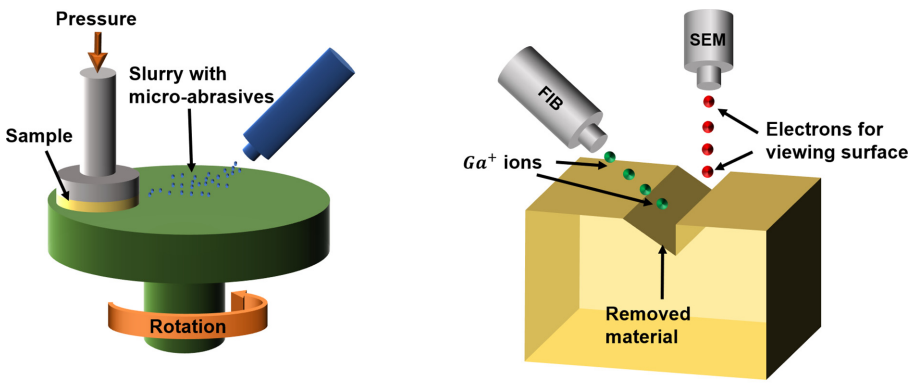

(a) Mechanical Polishing (b) Focused Ion Beam Milling

FIG. 1. Schematics of different methods for polishing microspheres: (a) mechanical polishing and (b) focused ion beam milling.

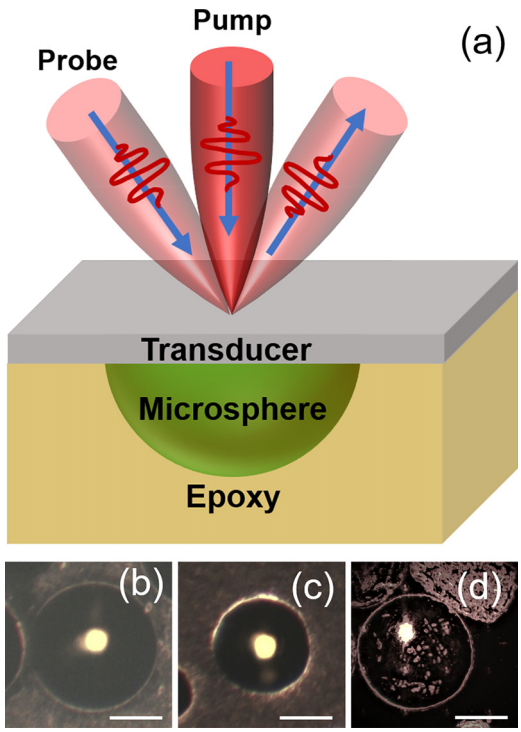

FIG. 2. (a) Schematic of the sample configuration for microspheres in TDTR measurements. Both pump and probe beams are focused on the polished microsphere surface. The CCD images of polished microspheres with probe beam illumination: (b) a glass sphere, (c) a YSZ sphere, and (d) an alumina sphere. Scale bars are 50 μm for all three spheres (b)–(d).

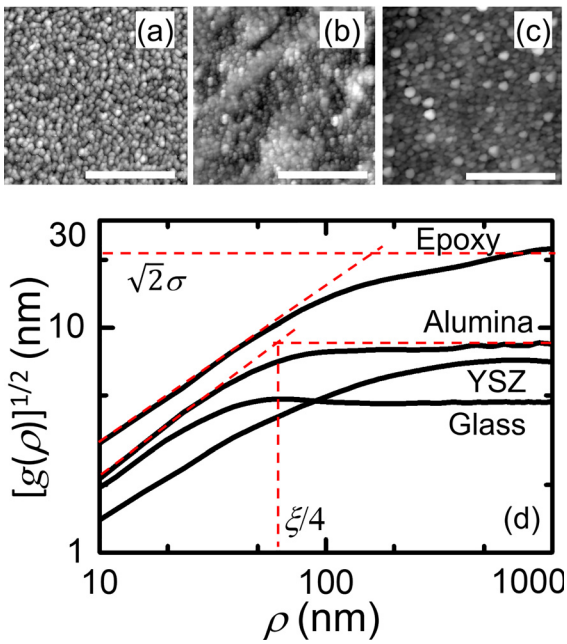

FIG. 3. AFM images of mechanically polished surfaces: (a) borosilicate glass, (b) YSZ, and (c) alumina. Scale bars are 1 μm. The height variation from black to white is ~20 nm for (a)–(c). (d) Square root of the height-difference correlation functions for mechanically polished surfaces for borosilicate glass, YSZ, alumina, and the epoxy matrix. Dashed lines show the intersection of the fittings for the linear and saturation regions, which is used to determine the correlation length.

microsphere, and the thermal anisotropy ($\eta = \Lambda_{in}/\Lambda$), defined as the ratio of the in-plane thermal conductivity to the through-plane thermal conductivity of the sample.[28,32] The glass microsphere is thermally isotropic due to its amorphous structure. For the YSZ and alumina microspheres, thermal transport is also isotropic resulting from the random orientations of polycrystalline domains in these microspheres. Thus, η is set as 1 for all three sample types. In fitting the TDTR measurement results to this thermal model, Λ and G are free parameters. Other parameters, such as h_{Al} and Λ_{Al} of the Al transducer layer, are determined from picosecond acoustics and the four-point probe method incorporated with the Wiedemann–Franz law. C_{Al} and C are taken from the literature. The model fitting is insensitive to the sample thickness since h is larger than the thermal penetration depth $[\delta = \sqrt{\Lambda/(\pi f C)}]$, which is estimated to be 150, 200, and 430 nm for the glass, YSZ, and alumina spheres, respectively.[33]

The surface morphologies of polished microspheres characterized with AFM are depicted in Figs. 3(a)–3(c), over a $2 \times 2\ \mu m^2$ scanned area. The height-difference correlation function $g(\rho)$ is used to analyze the sample surface features and is plotted in Fig. 3(d),

$$g(\rho) = \langle (h_i - h_j)^2 \rangle, \quad (1)$$

where h_i and h_j are the surface heights at location i and j, respectively, and ρ is the separation distance between these two locations. The brackets denote the ensemble average over such pairs of locations. For a separation distance ρ less than the correlation length ξ, $[g(\rho)]^{1/2}$ increases linearly with ρ, whereas for $\rho > \xi$, a saturation of $[g(\rho)]^{1/2}$ occurs, which approaches $\sqrt{2\sigma}$ with σ being the RMS surface roughness. The correlation length ξ can be identified via the intersection of the two fits for both the linear and saturated regions.[22] For all three types of microspheres, $[g(\rho)]^{1/2}$ is less than 10 nm, suggesting that the polished surfaces are sufficiently smooth for TDTR measurements.[34] The correlation lengths are approximately 80, 600, and 250 nm for glass, YSZ, and alumina microspheres, respectively, indicating the long-range surface uniformity of the samples. For comparison, the epoxy surface morphology is also measured with AFM and plotted in Fig. 3(d), which shows a larger $[g(\rho)]^{1/2}$ and, thus, a higher roughness. We speculate that this is attributed to the surface damage, such as scratches caused by polishing, or polishing residues that stick to the softer epoxy after the nitrogen cleaning process; however, such damage is unlikely to occur to the harder microspheres.

The polished sample surface produces a V_{dc} signal (proportional to the reflectivity from the sample) that is approximately 90% of the V_{dc} signal from a smooth SiO_2 reference coated with Al in the same sputtering chamber. This fact, along with the surface morphology features shown in Fig. 3, suggests that the polishing method implemented herein can serve as a high-throughput and relatively low-cost solution to prepare samples for studying the thermal properties of such microstructures embedded in a host medium with TDTR.

Alumina is an oxide that can exist in multiple phases depending on the processing methods, temperatures, and environments to which it has been exposed.[35] Transitional/metastable states of alumina are known to form as a result of pressure and heat treatment history.[36] The phases of alumina microspheres characterized with XRD are shown in Fig. 4(a). Based on automated reference-intensity-ratio analysis (Rigaku PDXL 2 software), the phases of alumina microspheres consist of α-phase and θ-phase alumina in composition percentages of ~85% and 15%, respectively. The density of alumina microspheres is also measured with a pycnometer, based on which, a porosity of 5% is estimated. A scanning electron microscopic image of unpolished alumina microspheres is shown in Fig. 4(b), suggesting a rough surface of these spheres likely resulting from their complex microstructures due to their processing history. We speculate that such structural features are also responsible for the difficulties encountered during polishing.

Figure 5(a) shows a representative picosecond acoustic signal from TDTR measurements of a YSZ microsphere. The first acoustic echo is reflected from the Al/YSZ interface, and its asymmetric shape is likely caused by a soft contamination layer between the YSZ microsphere and the Al transducer resulting from the polishing redidual.[33] Using the longitudinal speed of sound in Al and the time delay of the downward echo, the Al thickness is calculated as 69 ± 3 nm, close to that of the Al transducer for a SiO_2 reference from the same sputtering batch.[33] Similar echo features are also observed for glass and alumina microspheres. Figure 5(b) depicts the ratio signals for all three types of microspheres at dual modulation frequencies (9 and 18 MHz) with the best-fit curves calculated based on the thermal model.[28]

To ensure the measurement robustness, we carry out a sensitivity analysis to estimate the measurement sensitivity to individual parameters. It is found that the measurement is most sensitive to the volumetric heat capacity (C_{Al}) and thickness (h_{Al}) of the Al transducer, and

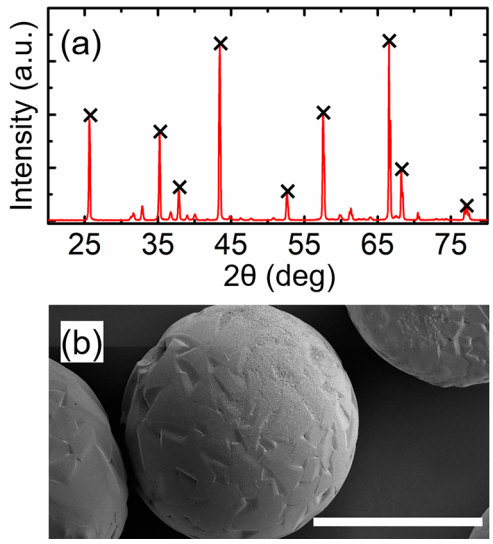

FIG. 4. (a) Phase composition of alumina microspheres from x-ray powder diffraction measurements. The "×" symbol indicates peaks correlating with α-alumina. All other features are attributable to the presence of metastable alumina phases, most notably, the θ-phase. (b) A scanning electron microscopic image (JEOL 6500F SEM) of unpolished alumina spheres. Scale bar in (b) is 100 μm.

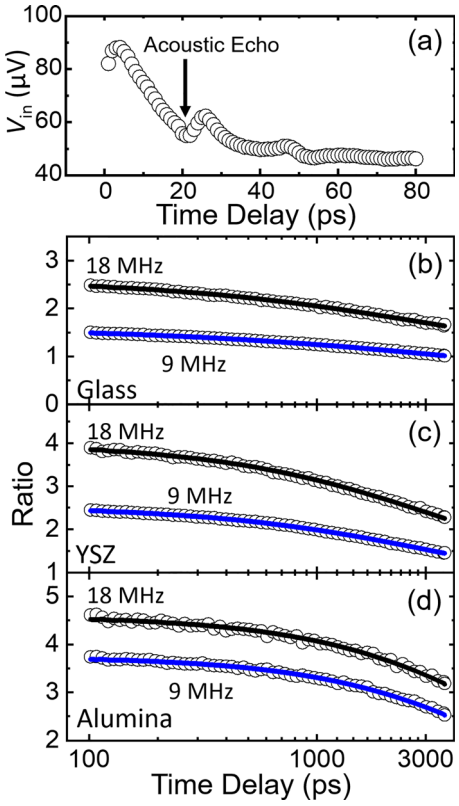

FIG. 5. (a) Representative in-phase signal of TDTR measurements on a YSZ microsphere, which illustrates the picosecond acoustic echoes resulting from the strain waves propagating in the Al transducer and getting reflected at the Al/YSZ interface. Representative ratio signals and corresponding dual-frequency fitting of glass (b), YSZ (c), and alumina (d) microspheres.

the thermal conductivity (Λ) and volumetric heat capacity (C) of the microspheres. The measurement is negligibly sensitive to the beam spot size (w_0) and the thermal conductivity of the transducer (Λ_{Al}). The measurements are also sensitive to the interfacial thermal conductance between the transducer and the microsphere (G) for the case of alumina microsphere due to its relatively high thermal conductivity compared with those of the YSZ and glass. The overall uncertainty of the sample thermal conductivity is obtained by combining the uncertainties propagated from individual fitting parameters in the thermal model with the standard deviation of measured thermal conductivities for multiple microspheres of the same type.[32]

The thermal conductivities from dual-frequency fitting are 1.17 ± 0.13 W m^{-1} K^{-1} for glass microspheres (averaged over three samples), 2.8 ± 0.31 W m^{-1} K^{-1} for YSZ microspheres (averaged over nine samples), and 15.8 ± 2.2 W m^{-1} K^{-1} for alumina microspheres (averaged over eight samples). For glass and YSZ microspheres with low thermal conductivities, thermal measurements are not sensitive enough to determine G. For alumina microspheres with relatively high thermal conductivities, the measured G values are $\sim 36 \pm 6.5$ MW m^{-2} K^{-1} This G value falls within the low thermal conductance category and is comparable to literature values of weak interfaces, suggesting possible surface contamination introduced during polishing processes. The

overall uncertainties are less than 15% for Λ of all three types of microspheres and ~20% for G of alumina microspheres.

Due to the amorphous nature of borosilicate glass, the thermal conductivity of glass microspheres is intrinsically low and does not show any size effect. Therefore, the thermal conductivity of glass microspheres measured with TDTR agrees well with literature values reported for bulk borosilicate glass.[37,38] For polycrystalline YSZ, the thermal conductivity depends significantly upon the concentration of yttria.[39–42] In crystalline solids, the primary heat carriers are phonons, which can be scattered by the structural disorders and/or defects, and, thus, reduce thermal transport.[39,43] In the case of zirconia and its alloys, the addition of yttria atoms as dopants can create oxygen vacancies. Both dopants and oxygen vacancies act as point defects in crystals, which can induce mass mismatch and localized strain fields affecting interatomic interactions (locally altering stiffness).[39] These imperfections enhance phonon scattering and reduces thermal conductivity. Thus, the thermal conductivity decreases as the yttria concentration increases in YSZ.[39] This dependence has been reported to result in the thermal conductivity of YSZ ranging from 1.5 to 3.5 W $m^{-1} K^{-1}$.[39–42] Our measured thermal conductivities of YSZ microspheres correspond to a molar concentration of ≈3% for yttria dopants. This is in good agreement with the yttria molar concentration (3.5%) of our YSZ microspheres determined from EDS measurements. It should be noted here that this ≈3% yttria molar concertation is a common alloy concentration for commercially available YSZ widely used in grinding media applications.[42]

Literature values for the thermal conductivity of alumina also vary greatly from 5 to 33 W $m^{-1} K^{-1}$ largely due to the phase contents and structural variations of samples prepared with different growth methods and corresponding heat and pressure treatments.[35,40,44] Considering the phase mixing and porous structural features of alumina microspheres, we apply an effective medium approximation (EMA) approach to interpret the thermal conductivity obtained from TDTR. The EMA has been widely used to calculate the effective thermal conductivity of composites with multi-phases and/or voids.[25,45] Several modified EMA approaches can further account for the interfacial thermal resistance between the filler and the matrix.[25,45] We choose the Bruggeman–Landauer (B–L) model as it is applicable for composites with high filler fractions, which is formulated as[45]

$$\sum_i f_i \frac{\Lambda_i - \Lambda_{\text{eff}}}{\Lambda_i + (n-1)\Lambda_{\text{eff}}} = 0, \tag{2}$$

where Λ_i and f_i are the thermal conductivity and fraction of individual components, Λ_{eff} is the effective thermal conductivity of the composite, and $n = 3$ is the spatial dimensions for alumina microspheres.[45] Using the thermal conductivities of α-phase (30 W $m^{-1} K^{-1}$) and θ-phase alumina (15 W $m^{-1} K^{-1}$) from the literature, the thermal conductivity of air (0.025 W $m^{-1} K^{-1}$),[35,44] and the volumetric fractions of alumina phases and pores, the B–L model predicts a value of 24 W $m^{-1} K^{-1}$ for Λ_{eff} of the alumina microsphere, nearly 50% higher than the measured thermal conductivity (15.8 W $m^{-1} K^{-1}$). One possible explanation for this discrepancy is because the B–L model only scales down the thermal conductivity based on material loss, but it does not consider changes in phonon scattering with voids and structural defects at differing length scales and with different defect densities. During the transition from θ-phase to α-phase alumina, it has been observed that vermicular crystal growth occurs.[36] This results in a large number of phase interfaces that create line and point defects in the crystal structure, which increase phonon scattering.[36] This scattering likely plays a significant role in reducing the effective thermal conductivity of the alumina microspheres compared with the B–L model prediction.

In summary, we have demonstrated a high-throughput method of sample preparation for direct thermal measurements of microspheres widely used as fillers for composite-based thermally conductive materials. The thermal conductivities of commercial glass and YSZ microspheres agree well with bulk values, as expected from the amorphous nature of glass microspheres and the fact that the micrometer sizes of crystalline YSZ spheres are much larger than the phonon mean free path in YSZ. We find that thermal transport in crystalline alumina microspheres is significantly suppressed, resulting from the enhanced phonon scattering with structural defects induced from phase mixing and porosity. Combining structural characterization and direct thermal measurements, our study provides insight into the fundamental thermal transport mechanisms in commercial microspheres as filler materials for developing composite-based materials for a wide range of thermal management applications.

This work was supported by the 3M Foundation. X.W.W. and Y.Y.Z. thank the support from the National Science Foundation (NSF, Award No. 1804840). Parts of the work were carried out in the Characterization Facility of the University of Minnesota, which is partially supported by the NSF through the MRSEC program (Award No. DMR-2011401).

DATA AVAILABILITY

The data that support the findings of this study are available within the article or from the corresponding author upon reasonable request.

REFERENCES

[1]Y. Cui, M. Li, and Y. J. Hu, J. Mater. Chem. C **8**(31), 10568–10586 (2020).
[2]S. Narumanchi, M. Mihalic, K. Kelly, and G. Eesley, Paper Presented at the Intersociety Conference on Thermal and Thermomechanical Phenomena in Electronic Systems XI, Orlando, FL, 2008.
[3]Z. L. Xiu, Y. Z. Wu, X. P. Hao, and L. Zhang, Colloid Surf. A **386**(1–3), 135–140 (2011).
[4]X. Y. Huang, C. Y. Zhi, and P. K. Jiang, J. Phys. Chem. C **116**(44), 23812–23820 (2012).
[5]M. Shtein, R. Nadiv, M. Buzaglo, K. Kahil, and O. Regev, Chem. Mater. **27**(6), 2100–2106 (2015).
[6]A. P. Yu, P. Ramesh, M. E. Itkis, E. Bekyarova, and R. C. Haddon, J. Phys. Chem. C **111**(21), 7565–7569 (2007).
[7]Y. F. Xu, X. J. Wang, and Q. Hao, Compos. Commun. **24**, 100617 (2021).
[8]D. W. Suh, C. M. Moon, D. J. Kim, and S. Y. Baik, Adv. Mater. **28**(33), 7220–7227 (2016).
[9]P. Zhang, J. H. Zeng, S. P. Zhai, Y. Q. Xian, D. G. Yang, and Q. Li, Macromol. Mater. Eng. **302**(9), 1700068 (2017).
[10]N. Burger, A. Laachachi, M. Ferriol, M. Lutz, V. Toniazzo, and D. Ruch, Prog. Polym. Sci. **61**, 1–28 (2016).
[11]H. K. Li and W. D. Zheng, J. Compos. Mater. **55**(1), 17–25 (2021).
[12]G. Droval, J.-F. Feller, P. Salagnac, and P. Glouannec, Polym. Adv. Technol. **17**(9–10), 732–745 (2006).
[13]R. A. Medina-Esquivel, M. A. Zambrano-Arjona, J. A. Mendez-Gamboa, J. M. Yanez-Limon, J. Ordonez-Miranda, and J. J. Alvarado-Gil, J. Appl. Phys. **111**(5), 054906 (2012).
[14]Z. D. Wang, Y. H. Cheng, H. K. Wang, M. M. Yang, Y. Y. Shao, X. Chen, and T. Tanaka, J. Mater. Sci. **52**(8), 4299–4308 (2017).
[15]W.-L. Ong, S. M. Rupich, D. V. Talapin, A. J. H. McGaughey, and J. A. Malen, Nat. Mater. **12**(5), 410–415 (2013).

[16]M. L. Liu, Y. Y. Ma, and R. Y. Wang, ACS Nano **9**(12), 12079–12087 (2015).
[17]A. Minnich and G. Chen, Appl. Phys. Lett. **91**(7), 073105 (2007).
[18]J. F. Wang, J. K. Carson, M. F. North, and D. J. Cleland, Int. J. Heat Mass Transfer **49**(17), 3075–3083 (2006).
[19]B. L. Liao and G. Chen, MRS Bull. **40**(9), 746–752 (2015).
[20]S. Ren, J. C. Liu, A. R. Guo, W. J. Zang, H. T. Geng, X. Tao, and H. Y. Du, Mater. Sci. Eng. A **674**, 604–614 (2016).
[21]F. Wang, X. Q. Qian, X. W. Li, J. K. Ye, Z. Han, Y. X. Chen, G. H. Liu, and J. T. Li, Mater. Lett. **151**, 82–84 (2015).
[22]X. J. Wang, V. Ho, R. A. Segalman, and D. G. Cahill, Macromolecules **46**(12), 4937 (2013).
[23]X. J. Wang, C. D. Liman, N. D. Treat, M. L. Chabinyc, and D. G. Cahill, Phys. Rev. B **88**(7), 075310 (2013).
[24]X. W. Wu, J. Walter, T. L. Feng, J. Zhu, H. Zheng, J. F. Mitchell, N. Biškup, M. Varela, X. L. Ruan, C. Leighton, and X. J. Wang, Adv. Funct. Mater. **27**(47), 1704233 (2017).
[25]X. W. Wu, B. L. Greenberg, Y. Y. Zhang, J. T. Held, D. B. Huang, J. G. Barriocanal, K. A. Mkhoyan, E. S. Aydil, U. Kortshagen, and X. J. Wang, Phys. Rev. Mater. **4**(8), 086001 (2020).
[26]Y. Y. Zhang, Q. Su, J. Zhu, S. Koirala, S. J. Koester, and X. J. Wang, Appl. Phys. Lett. **116**(20), 202101 (2020).
[27]J. Zhu, H. C. Park, J.-Y. Chen, X. K. Gu, H. Zhang, S. Karthikeyan, N. Wendel, S. A. Campbell, M. Dawber, X. Du, M. Li, J.-P. Wang, R. G. Yang, and X. J. Wang, Adv. Electron. Mater. **2**(5), 1600040 (2016).
[28]D. G. Cahill, Rev. Sci. Instrum. **75**(12), 5119–5122 (2004).
[29]R. Cheaito, J. T. Gaskins, M. E. Caplan, B. F. Donovan, B. M. Foley, A. Giri, J. C. Duda, C. J. Szwejkowski, C. Constantin, H. J. Brown-Shaklee, J. F. Ihlefeld, and P. E. Hopkins, Phys. Rev. B **91**(3), 035432 (2015).
[30]L. S. Larkin, J. L. Smoyer, and P. M. Norris, Int. J. Heat Mass Transfer **109**, 786–790 (2017).
[31]M. G. Burzo, P. L. Komarov, and P. E. Raad, IEEE Trans. Compon. Packag. Technol. **28**(1), 39–44 (2005).
[32]J. Zhu, X. W. Wu, D. M. Lattery, W. Zheng, and X. J. Wang, Nanoscale Microscale Thermophys. Eng. **21**(3), 177–198 (2017).
[33]G. T. Hohensee, W.-P. Hsieh, M. D. Losego, and D. G. Cahill, Rev. Sci. Instrum. **83**(11), 114902 (2012).
[34]T. Fu, Y. G. Shen, Z. F. Zhou, and K. Y. Li, Mater. Sci. Eng. B **123**(2), 158–162 (2005).
[35]N. Huda, M. A. Whitney, M. H. Razmpoosh, A. P. Gerlich, J. Z. Wen, and S. F. Corbin, J. Am. Ceram. Soc. **104**, 1436–1447 (2021).
[36]H.-C. Kao and W.-C. Wei, J. Am. Ceram. Soc. **83**(2), 362–368 (2004).
[37]H. Jena, R. Asuvathraman, K. V. G. Kutty, and P. R. V. Rao, J. Therm. Anal. Calorim. **115**(1), 367–374 (2014).
[38]M. J. Assael, S. Botsios, K. Gialou, and I. N. Metaxa, Int. J. Thermophys. **26**(5), 1595–1605 (2005).
[39]J. R. Nicholls, K. J. Lawson, A. Johnstone, and D. S. Rickerby, Surf. Coat. Technol. **151–152**, 383–391 (2002).
[40]D. G. Cahill, S. M. Lee, and T. I. Selinder, J. Appl. Phys. **83**(11), 5783–5786 (1998).
[41]G. Soyez, J. A. Eastman, L. J. Thompson, G. R. Bai, P. M. Baldo, A. W. McCormick, R. J. DiMelfi, A. A. Elmustafa, M. F. Tambwe, and D. S. Stone, Appl. Phys. Lett. **77**(8), 1155–1157 (2000).
[42]K. W. Schlichting, N. P. Padture, and P. G. Klemens, J. Mater. Sci. **36**(12), 3003–3010 (2001).
[43]G. Chen, *Nanoscale Energy Transport and Conversion: A Parallel Treatment of Electrons, Molecules, Phonons, and Photons* (Oxford University Press, Oxford, NY, 2005).
[44]I. Levin and D. Brandon, J. Am. Ceram. Soc. **81**(8), 1995–2012 (2005).
[45]S. P. Zhai, P. Zhang, Y. Q. Xian, J. H. Zeng, and B. Shi, Int. J. Heat Mass Transfer **117**, 358–374 (2018).